

## The Design and Performance of IceCube DeepCore

R. Abbasi<sup>ab</sup>, Y. Abdou<sup>v</sup>, T. Abu-Zayyad<sup>ag</sup>, M. Ackermann<sup>am</sup>, J. Adams<sup>p</sup>,  
 J. A. Aguilar<sup>ab</sup>, M. Ahlers<sup>af</sup>, M. M. Allen<sup>aj</sup>, D. Altmann<sup>a</sup>, K. Andeen<sup>ab,1</sup>,  
 J. Auffenberg<sup>al</sup>, X. Bai<sup>ae,2</sup>, M. Baker<sup>ab</sup>, S. W. Barwick<sup>x</sup>, R. Bay<sup>g</sup>,  
 J. L. Bazo Alba<sup>am</sup>, K. Beattie<sup>h</sup>, J. J. Beatty<sup>r,s</sup>, S. Bechet<sup>m</sup>, J. K. Becker<sup>j</sup>,  
 K.-H. Becker<sup>al</sup>, M. L. Benabderrahmane<sup>am</sup>, S. BenZvi<sup>ab</sup>, J. Berdermann<sup>am</sup>,  
 P. Berghaus<sup>ae</sup>, D. Berley<sup>q</sup>, E. Bernardini<sup>am</sup>, D. Bertrand<sup>m</sup>, D. Z. Besson<sup>z</sup>,  
 D. Bindig<sup>al</sup>, M. Bissok<sup>a</sup>, E. Blaufuss<sup>q</sup>, J. Blumenthal<sup>a</sup>, D. J. Boersma<sup>a</sup>,  
 C. Boehm<sup>ah</sup>, D. Bose<sup>n</sup>, S. Böser<sup>k</sup>, O. Botner<sup>ak</sup>, A. M. Brown<sup>p</sup>, S. Buitink<sup>n</sup>,  
 K. S. Caballero-Mora<sup>aj</sup>, M. Carson<sup>v</sup>, D. Chirkin<sup>ab</sup>, B. Christy<sup>q</sup>,  
 F. Clevermann<sup>t</sup>, S. Cohen<sup>y</sup>, C. Colnard<sup>w</sup>, D. F. Cowen<sup>aj,ai</sup>,  
 A. H. Cruz Silva<sup>am</sup>, M. V. D'Agostino<sup>g</sup>, M. Danninger<sup>ah</sup>, J. Daughhetee<sup>e</sup>,  
 J. C. Davis<sup>r</sup>, C. De Clercq<sup>n</sup>, T. Degner<sup>k</sup>, L. Demirörs<sup>y</sup>, F. Descamps<sup>v</sup>,  
 P. Desiati<sup>ab</sup>, G. de Vries-Uiterweerd<sup>v</sup>, T. DeYoung<sup>aj</sup>, J. C. Díaz-Vélez<sup>ab</sup>,  
 M. Dierckxsens<sup>m</sup>, J. Dreyer<sup>j</sup>, J. P. Dumm<sup>ab</sup>, M. Dunkman<sup>aj</sup>, J. Eisch<sup>ab</sup>,  
 R. W. Ellsworth<sup>q</sup>, O. Engdegård<sup>ak</sup>, S. Euler<sup>a</sup>, P. A. Evenson<sup>ae</sup>, O. Fadiran<sup>ab</sup>,  
 A. R. Fazely<sup>f</sup>, A. Fedynitch<sup>j</sup>, J. Feintzeig<sup>ab</sup>, T. Feusels<sup>v</sup>, K. Filimonov<sup>g</sup>,  
 C. Finley<sup>ah</sup>, T. Fischer-Wasels<sup>al</sup>, B. D. Fox<sup>aj</sup>, A. Franckowiak<sup>k</sup>, R. Franke<sup>am</sup>,  
 T. K. Gaisser<sup>ae</sup>, J. Gallagher<sup>aa</sup>, L. Gerhardt<sup>h,g</sup>, L. Gladstone<sup>ab</sup>,  
 T. Glüsenskamp<sup>am</sup>, A. Goldschmidt<sup>h</sup>, J. A. Goodman<sup>q</sup>, D. Góra<sup>am</sup>, D. Grant<sup>u</sup>,  
 T. Griesel<sup>ac</sup>, A. Groß<sup>p,w</sup>, S. Grullon<sup>ab</sup>, M. Gurtner<sup>al</sup>, C. Ha<sup>aj</sup>, A. Haj Ismail<sup>v</sup>,  
 A. Hallgren<sup>ak</sup>, F. Halzen<sup>ab</sup>, K. Han<sup>am</sup>, K. Hanson<sup>m,ab</sup>, D. Heinen<sup>a</sup>,  
 K. Helbing<sup>al</sup>, R. Hellauer<sup>q</sup>, S. Hickford<sup>p</sup>, G. C. Hill<sup>ab</sup>, K. D. Hoffman<sup>q</sup>,  
 B. Hoffmann<sup>a</sup>, A. Homeier<sup>k</sup>, K. Hoshina<sup>ab</sup>, W. Huelsnitz<sup>q,3</sup>, J.-P. Hülß<sup>a</sup>,  
 P. O. Hulth<sup>ah</sup>, K. Hultqvist<sup>ah</sup>, S. Hussain<sup>ae</sup>, A. Ishihara<sup>o</sup>, E. Jacobi<sup>am</sup>,  
 J. Jacobsen<sup>ab</sup>, G. S. Japaridze<sup>d</sup>, H. Johansson<sup>ah</sup>, K.-H. Kampert<sup>al</sup>,  
 A. Kappes<sup>i</sup>, T. Karg<sup>al</sup>, A. Karle<sup>ab</sup>, P. Kenny<sup>z</sup>, J. Kiryluk<sup>h,g</sup>, F. Kislak<sup>am</sup>,  
 S. R. Klein<sup>h,g</sup>, J.-H. Köhne<sup>t</sup>, G. Kohnen<sup>ad</sup>, H. Kolanoski<sup>i</sup>, L. Köpke<sup>ac</sup>,  
 S. Kopper<sup>al</sup>, D. J. Koskinen<sup>aj</sup>, M. Kowalski<sup>k</sup>, T. Kowarik<sup>ac</sup>, M. Krasberg<sup>ab</sup>,  
 G. Kroll<sup>ac</sup>, N. Kurahashi<sup>ab</sup>, T. Kuwabara<sup>ae</sup>, M. Labare<sup>n</sup>, K. Laihem<sup>a</sup>,  
 H. Landsman<sup>ab</sup>, M. J. Larson<sup>aj</sup>, R. Lauer<sup>am</sup>, J. Lünemann<sup>ac</sup>, J. Madsen<sup>ag</sup>,  
 A. Marotta<sup>m</sup>, R. Maruyama<sup>ab</sup>, K. Mase<sup>o</sup>, H. S. Matis<sup>h</sup>, K. Meagher<sup>q</sup>,  
 M. Merck<sup>ab</sup>, P. Mészáros<sup>ai,aj</sup>, T. Meures<sup>m</sup>, S. Miarecki<sup>h,g</sup>, E. Middell<sup>am</sup>,  
 N. Milke<sup>t</sup>, J. Miller<sup>ak</sup>, T. Montaruli<sup>ab,4</sup>, R. Morse<sup>ab</sup>, S. M. Movit<sup>ai</sup>,  
 R. Nahnauer<sup>am</sup>, J. W. Nam<sup>x</sup>, U. Naumann<sup>al</sup>, D. R. Nygren<sup>h</sup>, S. Odrowski<sup>w</sup>,

<sup>1</sup>Now at Dept. of Physics and Astronomy, Rutgers University, Piscataway, NJ 08854, USA

<sup>2</sup>Now at Physics Department, South Dakota School of Mines and Technology, Rapid City, SD 57701, USA

<sup>3</sup>Los Alamos National Laboratory, Los Alamos, NM 87545, USA

<sup>4</sup>Also Sezione INFN, Dipartimento di Fisica, I-70126, Bari, Italy

<sup>5</sup>Now at T.U. Munich, 85748 Garching & Friedrich-Alexander Universität Erlangen-Nürnberg, 91058 Erlangen, Germany

<sup>6</sup>Now at T.U. Munich, 85748 Garching, Germany

<sup>7</sup>NASA Goddard Space Flight Center, Greenbelt, MD 20771, USA

A. Olivas<sup>q</sup>, M. Olivo<sup>j</sup>, A. O’Murchadha<sup>ab</sup>, S. Panknin<sup>k</sup>, L. Paul<sup>a</sup>,  
C. Pérez de los Heros<sup>ak</sup>, J. Petrovic<sup>m</sup>, A. Piegsa<sup>ac</sup>, D. Pieloth<sup>t</sup>, R. Porrata<sup>g</sup>,  
J. Posselt<sup>al</sup>, P. B. Price<sup>g</sup>, G. T. Przybylski<sup>h</sup>, K. Rawlins<sup>c</sup>, P. Redl<sup>q</sup>,  
E. Resconi<sup>w,5</sup>, W. Rhode<sup>t</sup>, M. Ribordy<sup>y</sup>, M. Richman<sup>q</sup>, J. P. Rodrigues<sup>ab</sup>,  
F. Rothmaier<sup>ac</sup>, C. Rott<sup>f</sup>, T. Ruhe<sup>t</sup>, D. Rutledge<sup>aj</sup>, B. Ruzybayev<sup>ae</sup>,  
D. Ryckbosch<sup>v</sup>, H.-G. Sander<sup>ac</sup>, M. Santander<sup>ab</sup>, S. Sarkar<sup>af</sup>, K. Schatto<sup>ac</sup>,  
T. Schmidt<sup>q</sup>, A. Schönwald<sup>am</sup>, A. Schukraft<sup>a</sup>, A. Schultes<sup>al</sup>, O. Schulz<sup>w,6</sup>,  
M. Schunck<sup>a</sup>, D. Seckel<sup>ae</sup>, B. Semburg<sup>al</sup>, S. H. Seo<sup>ah</sup>, Y. Sestayo<sup>w</sup>,  
S. Seunarine<sup>l</sup>, A. Silvestri<sup>x</sup>, G. M. Spiczak<sup>ag</sup>, C. Spiering<sup>am</sup>, M. Stamatikos<sup>r,7</sup>,  
T. Stanev<sup>ae</sup>, T. Stezelberger<sup>h</sup>, R. G. Stokstad<sup>h</sup>, A. Stöbl<sup>am</sup>, E. A. Strahler<sup>n</sup>,  
R. Ström<sup>ak</sup>, M. Stüer<sup>k</sup>, G. W. Sullivan<sup>q</sup>, Q. Swillens<sup>m</sup>, H. Taavola<sup>ak</sup>,  
I. Taboada<sup>e</sup>, A. Tamburro<sup>ag</sup>, A. Tepe<sup>e</sup>, S. Ter-Antonyan<sup>f</sup>, S. Tilav<sup>ae</sup>,  
P. A. Toale<sup>b</sup>, S. Toscano<sup>ab</sup>, D. Tosi<sup>am</sup>, N. van Eijndhoven<sup>n</sup>,  
J. Vandenbroucke<sup>g</sup>, A. Van Overloop<sup>v</sup>, J. van Santen<sup>ab</sup>, M. Vehring<sup>a</sup>,  
M. Voge<sup>k</sup>, C. Walck<sup>ah</sup>, T. Waldenmaier<sup>i</sup>, M. Wallraff<sup>a</sup>, M. Walter<sup>am</sup>,  
Ch. Weaver<sup>ab</sup>, C. Wendt<sup>ab</sup>, S. Westerhoff<sup>ab</sup>, N. Whitehorn<sup>ab</sup>, K. Wiebe<sup>ac</sup>,  
C. H. Wiebusch<sup>a</sup>, D. R. Williams<sup>b</sup>, R. Wischnewski<sup>am</sup>, H. Wissing<sup>q</sup>, M. Wolf<sup>w</sup>,  
T. R. Wood<sup>u</sup>, K. Woschnagg<sup>g</sup>, C. Xu<sup>ae</sup>, D. L. Xu<sup>b</sup>, X. W. Xu<sup>f</sup>, J. P. Yanez<sup>am</sup>,  
G. Yodh<sup>x</sup>, S. Yoshida<sup>o</sup>, P. Zarzhitsky<sup>b</sup>, M. Zoll<sup>ah</sup>

<sup>a</sup>III. Physikalisches Institut, RWTH Aachen University, D-52056 Aachen, Germany

<sup>b</sup>Dept. of Physics and Astronomy, University of Alabama, Tuscaloosa, AL 35487, USA

<sup>c</sup>Dept. of Physics and Astronomy, University of Alaska Anchorage, 3211 Providence Dr., Anchorage, AK 99508, USA

<sup>d</sup>CTSPS, Clark-Atlanta University, Atlanta, GA 30314, USA

<sup>e</sup>School of Physics and Center for Relativistic Astrophysics, Georgia Institute of Technology, Atlanta, GA 30332, USA

<sup>f</sup>Dept. of Physics, Southern University, Baton Rouge, LA 70813, USA

<sup>g</sup>Dept. of Physics, University of California, Berkeley, CA 94720, USA

<sup>h</sup>Lawrence Berkeley National Laboratory, Berkeley, CA 94720, USA

<sup>i</sup>Institut für Physik, Humboldt-Universität zu Berlin, D-12489 Berlin, Germany

<sup>j</sup>Fakultät für Physik & Astronomie, Ruhr-Universität Bochum, D-44780 Bochum, Germany

<sup>k</sup>Physikalisches Institut, Universität Bonn, Nussallee 12, D-53115 Bonn, Germany

<sup>l</sup>Dept. of Physics, University of the West Indies, Cave Hill Campus, Bridgetown BB11000, Barbados

<sup>m</sup>Université Libre de Bruxelles, Science Faculty CP230, B-1050 Brussels, Belgium

<sup>n</sup>Vrije Universiteit Brussel, Dienst ELEM, B-1050 Brussels, Belgium

<sup>o</sup>Dept. of Physics, Chiba University, Chiba 263-8522, Japan

<sup>p</sup>Dept. of Physics and Astronomy, University of Canterbury, Private Bag 4800, Christchurch, New Zealand

<sup>q</sup>Dept. of Physics, University of Maryland, College Park, MD 20742, USA

<sup>r</sup>Dept. of Physics and Center for Cosmology and Astro-Particle Physics, Ohio State University, Columbus, OH 43210, USA

<sup>s</sup>Dept. of Astronomy, Ohio State University, Columbus, OH 43210, USA

<sup>t</sup>Dept. of Physics, TU Dortmund University, D-44221 Dortmund, Germany

<sup>u</sup>Dept. of Physics, University of Alberta, Edmonton, Alberta, Canada T6G 2G7

<sup>v</sup>Dept. of Physics and Astronomy, University of Gent, B-9000 Gent, Belgium

<sup>w</sup>Max-Planck-Institut für Kernphysik, D-69177 Heidelberg, Germany

<sup>x</sup>Dept. of Physics and Astronomy, University of California, Irvine, CA 92697, USA

<sup>y</sup>Laboratory for High Energy Physics, École Polytechnique Fédérale, CH-1015 Lausanne, Switzerland

<sup>z</sup>Dept. of Physics and Astronomy, University of Kansas, Lawrence, KS 66045, USA

<sup>aa</sup>Dept. of Astronomy, University of Wisconsin, Madison, WI 53706, USA

<sup>ab</sup>*Dept. of Physics, University of Wisconsin, Madison, WI 53706, USA*  
<sup>ac</sup>*Institute of Physics, University of Mainz, Staudinger Weg 7, D-55099 Mainz, Germany*  
<sup>ad</sup>*Université de Mons, 7000 Mons, Belgium*  
<sup>ae</sup>*Bartol Research Institute and Department of Physics and Astronomy, University of Delaware, Newark, DE 19716, USA*  
<sup>af</sup>*Dept. of Physics, University of Oxford, 1 Keble Road, Oxford OX1 3NP, UK*  
<sup>ag</sup>*Dept. of Physics, University of Wisconsin, River Falls, WI 54022, USA*  
<sup>ah</sup>*Oskar Klein Centre and Dept. of Physics, Stockholm University, SE-10691 Stockholm, Sweden*  
<sup>ai</sup>*Dept. of Astronomy and Astrophysics, Pennsylvania State University, University Park, PA 16802, USA*  
<sup>aj</sup>*Dept. of Physics, Pennsylvania State University, University Park, PA 16802, USA*  
<sup>ak</sup>*Dept. of Physics and Astronomy, Uppsala University, Box 516, S-75120 Uppsala, Sweden*  
<sup>al</sup>*Dept. of Physics, University of Wuppertal, D-42119 Wuppertal, Germany*  
<sup>am</sup>*DESY, D-15735 Zeuthen, Germany*

---

## Abstract

The IceCube neutrino observatory in operation at the South Pole, Antarctica, comprises three distinct components: a large buried array for ultrahigh energy neutrino detection, a surface air shower array, and a new buried component called DeepCore. DeepCore was designed to lower the IceCube neutrino energy threshold by over an order of magnitude, to energies as low as about 10 GeV. DeepCore is situated primarily 2100 m below the surface of the icecap at the South Pole, at the bottom center of the existing IceCube array, and began taking physics data in May 2010. Its location takes advantage of the exceptionally clear ice at those depths and allows it to use the surrounding IceCube detector as a highly efficient active veto against the principal background of downward-going muons produced in cosmic-ray air showers. DeepCore has a module density roughly five times higher than that of the standard IceCube array, and uses photomultiplier tubes with a new photocathode featuring a quantum efficiency about 35% higher than standard IceCube PMTs. Taken together, these features of DeepCore will increase IceCube’s sensitivity to neutrinos from WIMP dark matter annihilations, atmospheric neutrino oscillations, galactic supernova neutrinos, and point sources of neutrinos in the northern and southern skies. In this paper we describe the design and initial performance of DeepCore.

---

## 1. Introduction

DeepCore is a new subarray of the IceCube observatory [1] that was designed to provide sensitivity to neutrinos at energies over an order of magnitude lower than initially envisioned for the original array. Using the Cherenkov light emitted by charged particles arising from neutrino interactions in the ice, the subarray achieves this improved sensitivity through a combination of increased

module density, higher quantum efficiency photomultiplier tubes (PMTs), deployment in the clearest ice at depths greater than 2100 m, and use of the surrounding standard IceCube modules above and around DeepCore as a powerful active veto against the copious downward-going cosmic-ray muon background.

DeepCore provides enhanced sensitivity to weakly interacting massive particles (WIMPs) and is expected to significantly improve existing IceCube results on WIMP annihilations in the Sun [2], Galactic Center [3] and Halo [4], extending limits below present accelerator bounds. DeepCore gives improved acceptance for low energy atmospheric neutrinos at  $E_\nu \gtrsim 10$  GeV, opening a useful new window for atmospheric neutrino oscillation measurements, including  $\nu_\mu$  disappearance,  $\nu_\tau$  appearance and as a remote possibility, the sign of the neutrino hierarchy [5]. Taking advantage of the active vetoing capability provided by the surrounding IceCube array, DeepCore allows us to explore the southern sky for diffuse and point source neutrino emission from active galactic nuclei (AGN), gamma ray bursts (GRBs), choked GRBs [6], and the inner galaxy. The increased module density of DeepCore may enable the reconstruction of more closely-spaced cascades produced by an initial  $\nu_\tau$  interaction and the subsequent  $\tau$  decay, extending the search for cosmological  $\nu_\tau$  to lower energies. The higher module density may also enable the reconstruction of the average energy of galactic supernova neutrinos [7, 8]. Searches for slow-moving monopoles, supersymmetric stau pair production [9, 10] and low-energy neutrino emission from astrophysical sources [11] will likewise benefit from DeepCore’s extension of IceCube’s capabilities.

Section 2 of this paper describes the design of DeepCore, highlighting the geometrical layout of the sub-array of digital optical modules (DOMs) that house the PMTs and their associated readout electronics [12, 13], the optical quality of the ice in which DeepCore has been deployed, the performance characteristics of its high quantum efficiency PMTs, and the schedule for DeepCore deployment that led to “first light” in mid-2010. In Section 3 we describe the results of simulations performed with IceCube and DeepCore, showing predicted triggering and quasi-real-time event selection (“filtering”) performance, and estimations of neutrino effective volumes. Section 4 gives our conclusions.

## 2. DeepCore Design and Schedule

### 2.1. Ice Properties

The Antarctic Muon and Neutrino Detector Array (AMANDA, the predecessor to IceCube) was used to map [14] the relevant wavelength and depth dependence of light absorption and scattering down to a depth of 2350 m, albeit with poor precision beyond 2100 m because of much sparser instrumentation in the deepest ice. Variations with depth in the optical ice properties were found to closely track concentrations in mineral dust deposits which in turn are correlated with climatological history. Dust concentrations are the highest in a depth band between 2000 and 2100 m, here denoted the “dust layer,” corresponding to a stadial about 65,000 years ago, in the last glacial period. DeepCore was designed to avoid this highly absorbing and scattering ice.

Our knowledge of the optical properties of the ice in which DeepCore is located has been augmented more recently with *in situ* measurements using pulsed LED sources in IceCube. These preliminary time-of-flight measurements verify that the ice at depths greater than 2100 m is significantly more transparent optically than the shallower ice between 1500 and 2000 m. We also see this qualitatively in IceCube data from downward-going muons, which show a strong light depletion in the dust layer followed by increased light yield at greater depths (see Fig. 5).

In terms of scattering and absorption lengths, the parameters describing photon propagation that need to be known to simulate (see Sec. 3.1) and reconstruct neutrino-induced events, the average ice at depths below 2100 m is estimated to be about 40%-50% clearer than the ice between 1500 and 2000 m. In the clearest ice, around 2400 m depth, the average effective scattering length is close to 50 m and the average absorption length is close to 190 m. These values are for 400 nm light, the wavelength where absorption due to dust is weakest and the ice is most transparent. This wavelength is also near the peak of the DOM sensitivity [12].

## 2.2. Photomultiplier Tubes

The photomultiplier tube used in the standard IceCube DOMs is the Hamamatsu 252 mm diameter R7081-02 [12]. During the planning for DeepCore, Hamamatsu presented a new version of the PMT, the R7081MOD, with higher quantum efficiency. The R7081MOD is identical to the standard IceCube PMT, but with a “super bialkali” photocathode that improves the quantum efficiency by about 40% at photon wavelength  $\lambda = 390$  nm in laboratory measurements performed by Hamamatsu. Eight of these new PMTs were tested in the laboratory by IceCube, confirming the higher quantum efficiency. Subsequent simulations demonstrated that the added efficiency would increase the effective area of DeepCore for triggering on low energy neutrinos by about 30%. All DOMs equipped with the new high quantum efficiency PMTs (“HQE DOMs”) were fully tested in the standard IceCube DOM testing system and the results from the first 80 of these are compared with the standard DOMs in Figs. 1, 2 and 3. These tests included several temperature cycles from  $+25^\circ\text{C}$  to  $-45^\circ\text{C}$  to simulate the temperatures the DOMs would experience during transportation and deployment. Once deployed, the ambient temperature varies between approximately  $-45^\circ\text{C}$  to  $-20^\circ\text{C}$ , becoming warmer with increasing depth. [15]

In the laboratory measurements the HQE DOMs showed a 39% higher optical sensitivity than standard DOMs at  $\lambda = 405$  nm (Fig. 1). An *in-situ* measurement showed an improvement of about 35%, smaller than the laboratory measurements and possibly due to the non-monochromatic Cherenkov spectrum and to the different optical system created by the surrounding ice. Additional properties of the HQE DOMs that differ from those of standard DOMs include: an average noise rate that is higher by a factor of 1.33 at  $-45^\circ\text{C}$  and with a programmable deadtime set to 100 ns (Fig. 2); a high voltage at  $10^7$  gain that is 100 V lower; and a slightly larger peak-to-valley ratio. Standard and HQE DOMs exhibited similar photo-electron pulse height and charge spectra (Fig. 3).

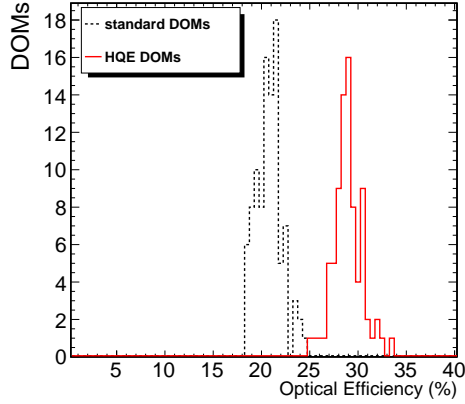


Figure 1: Laboratory measurement of the relative optical efficiencies at  $-45^{\circ}\text{C}$  and 405 nm, near the peak PMT sensitivity. A standard reference 2-inch PMT was used for normalization purposes. The black dashed curve is for DOMs with standard PMTs, the red solid curve for HQE DOMs. Using the ratio of the mean relative efficiencies, the new PMTs have an efficiency 1.39 times higher than the standard PMTs.

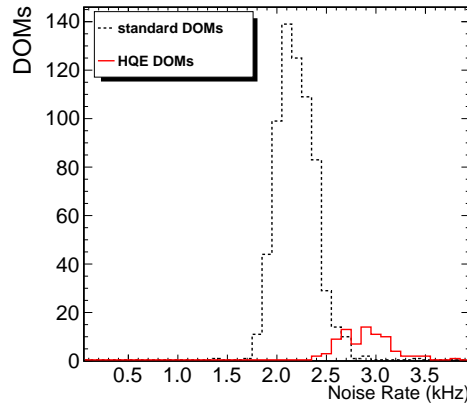


Figure 2: Laboratory measurement of the HQE DOM noise rate for the DOM at  $-45^{\circ}\text{C}$ . The black dashed curve is for DOMs with standard PMTs, the red solid curve for HQE DOMs.

Figure 4 shows the dark noise rates and Fig. 5 shows the relative occupancies for standard and HQE DOMs, measured *in situ*. The occupancy is defined as the fraction of events in which each DOM detected one or more photons and is on a string with at least seven other DOMs that also detected photons. Each DOM must also be in “hard local coincidence,” a condition that requires it to have at least one neighboring DOM registering a hit contemporaneously (see

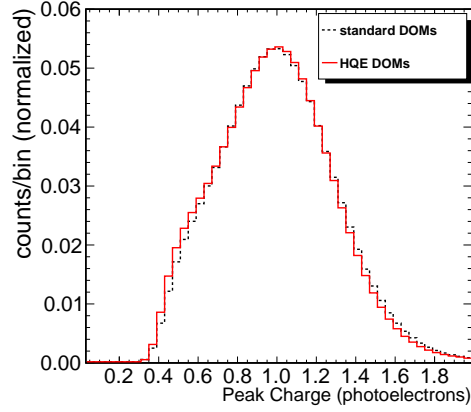


Figure 3: Laboratory measurement of the HQE DOM charge response for the DOM at  $-45^{\circ}\text{C}$ . The black dashed curve is for DOMs with standard PMTs, the red solid curve for HQE DOMs.

Sec. 3.1).

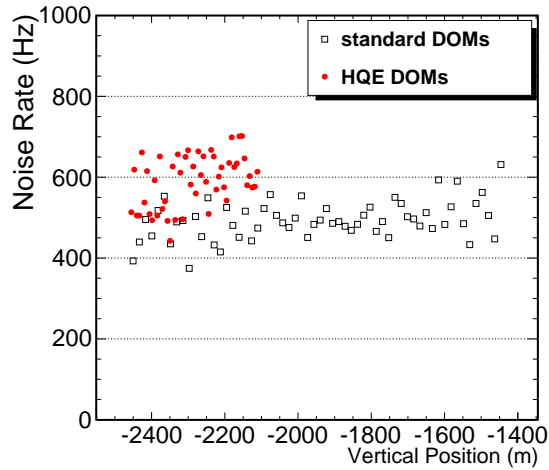


Figure 4: HQE DOM noise rates from *in situ* measurements as a function of deployment depth. The black squares are for DOMs with standard PMTs, the red circles for HQE DOMs. The higher noise rate is consistent with the increased quantum efficiency.

### 2.3. Geometry

The geometric parameters that directly impact the ability of DeepCore to reconstruct low energy events and discriminate them from the cosmic-ray muon

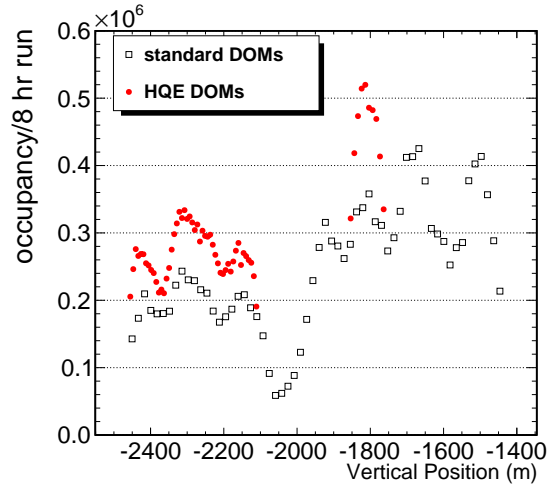


Figure 5: HQE DOM occupancies (defined in the text) from *in situ* measurements as a function of deployment depth. The black squares are for standard PMTs, the red circles are for HQE PMTs. The latter show a higher occupancy due to improved quantum efficiency.

background are its horizontal string-to-string and vertical DOM-to-DOM spacings. Since low energy muons ( $E_\mu \sim 1$  TeV) in ice travel about 5 m per GeV of energy, the 125 m horizontal string spacing and 17 m vertical DOM spacing of the baseline IceCube detector translate to a minimum neutrino energy threshold for most analyses of about 50–100 GeV, and an optimal response at  $E_\nu \gtrsim 1$  TeV.

Low energy events are especially susceptible to background contamination from atmospheric cosmic-ray muons. Cosmic-ray muons trigger IceCube at a rate approximately  $10^6$  times higher than atmospheric neutrino interactions in the detector. The flux of these background events is greater at lower energies, and the ability to distinguish between signal and background is more challenging in events with low light levels. The muon background is suppressed both by situating DeepCore at the greatest available depths and by using the entire surrounding IceCube detector as an active veto. Most downward-going cosmic-ray muons are unlikely to evade detection by the large number of surrounding DOMs before entering the DeepCore’s 125 m radius by 350 m long cylindrical fiducial volume.

The DeepCore geometry was optimized using a Monte Carlo (MC) simulation based on the detailed simulation tools already in use by IceCube. The emphasis was on maximizing the detection efficiency for fully or partially contained (i.e., starting) neutrino events in the 10–100 GeV energy range while also achieving cosmic-ray background rejection of  $10^6$  or better. For reference, fully-contained upward-going muons with  $E_\mu \simeq 10$  GeV can illuminate about 10 DOMs in DeepCore, a number sufficient both for triggering the detector and



for applying sophisticated reconstruction algorithms.

We varied DOM and inter-string spacing, balancing the competing advantages of higher module density and greater fiducial volume, while remaining consistent with drilling and down-hole cable breakout constraints. The chosen configuration (see Fig. 6) comprises eight new strings, six with 60 HQE DOMs, located very near the bottom center of IceCube, logically joined with the bottom third of the seven nearest-neighbor standard IceCube strings. The average inter-string horizontal distance between 13 of the 15 DeepCore strings is 72 m, about 1.5 times the effective scattering length of the ice surrounding most of DeepCore. For six of the 15 DeepCore strings, the interstring spacing is 42 m. On each new string, 50 DOMs with 7 m vertical spacing are located in the deepest ice instrumented by IceCube, between 2100 and 2450 m below the surface of the polar icecap, where the scattering and absorption lengths are substantially longer than at shallower depths. The region between 2000 and 2100 m depths is not instrumented with DeepCore DOMs due to the significant scattering and absorption of light that occurs there. Instead, the remaining 10 DOMs of each of the eight high-density DeepCore strings are placed directly above this region with a spacing of 10 m, providing an added overhead veto “plug” to further enhance background rejection from the vertical direction where the cosmic-ray angular distribution is peaked. These remaining DOMs also improve the reconstruction of low-energy, near-horizontal tracks useful in certain ongoing analyses.

The first specialized DeepCore string was successfully deployed in January 2009 [16]. In addition, six of the seven standard IceCube strings that are part of the DeepCore fiducial volume were deployed. In the following 2009/2010 austral summer season, the five remaining DeepCore strings with HQE PMTs and the one remaining standard IceCube string were deployed. At that point, DeepCore was comprised of six strings with closely spaced HQE-PMT DOMs and seven standard IceCube strings, and was fully surrounded by three layers of standard IceCube strings. This DeepCore configuration started acquiring physics data in April 2010.

The two DeepCore strings on 42 m horizontal spacing were deployed in the 2010/2011 austral summer. Initial MC studies have shown that this closer-packed configuration will further improve DeepCore’s low energy response, with an estimated 30% increased rate for events with  $E_\nu = 10 - 20$  GeV having six or more hits in the fiducial volume.

### 3. Simulation and Selection of DeepCore Events

#### 3.1. Simulation Tools

Monte Carlo studies have been used to design DeepCore and optimize its geometry, to study the signal acceptance and background veto efficiency, and to evaluate its physics potential. The MC data for all these studies were generated using the complete IceCube simulation package, called IceSim. IceSim has interfaces to various programs needed to produce the signal and background events

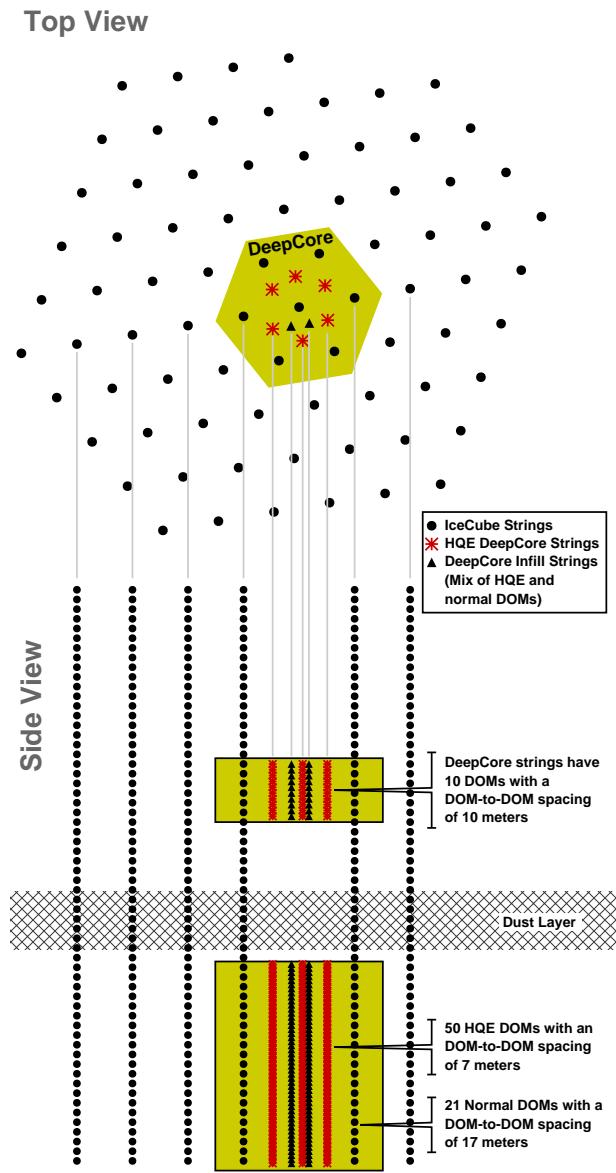


Figure 6: A schematic layout of IceCube DeepCore. The upper diagram shows a top view of the string positions in relation to current and future IceCube strings. It includes two additional strings, situated close to the central DeepCore string, that were deployed in the 2010/2011 austral summer. Please see the text for a quantitative description of the detector geometry.

of interest. Atmospheric muons were simulated with an air shower simulation program CORSIKA (COsmic Ray SIMulation KAscade) [17] and neutrinos were generated with code based on ANIS (All Neutrino Interaction Generator) [18] and with GENIE (Generates Events for Neutrino Interaction Experiments) [19]. Originally developed for the AMANDA detector and recently adapted for use in the IceCube software framework, ANIS is capable of generating neutrinos with energies between 10 GeV and 1 ZeV. With a more accurate description of neutrino interactions below  $E_\nu = 10$  GeV, GENIE is a state-of-the-art generator used in the broader neutrino community, in particular by accelerator neutrino experiments, and has been extensively verified. It is foreseen that an extension of GENIE to higher energies will become available in the near future, covering the full IceCube detector energy range.

In each of these programs a parent particle was produced and propagated to a specific boundary of the detector geometry. For instance, the CORSIKA-generated cosmic-ray muons were propagated to the surface of the earth, and ANIS-generated neutrinos to a cylinder of fixed radius around the IceCube detector. Once the parent particle reached the boundary, its charged lepton daughters were propagated with MMC [20], also interfaced with IceSim.

IceSim contains the full details of the IceCube detector, including DOM hardware and firmware simulation and Photonics [21] which propagates photons emitted by charged particle interactions through the ice, taking into account local variations in its optical properties [14]. This simulation chain, from parent particles to the leptons and photons and finally to a DOM/PMT simulation, produces simulated events containing the list of hit DOMs with associated charge and timing. The content of the simulation output is a superset of that produced by the IceCube detector DAQ. The same trigger, filter and analysis algorithms are applied to both simulated and real data.

IceSim's modular design made the inclusion of DeepCore straightforward. The main difference was the higher average noise rate and improved photon detection efficiency of the HQE DOMs. To account for these differences in these initial studies, estimated linear scale factors were introduced, based on preliminary lab measurements of the HQE DOMs. The simulated noise rate was increased by a factor of 1.54 and the PMT quantum efficiency was increased by a factor of 1.25 relative to standard DOMs. (As shown in Sec. 2.2, later measurements of the noise rate and relative quantum efficiency indicate that these estimates were approximately correct.) Eventually, the relative quantum efficiency for these DOMs, which is wavelength dependent, will be included directly in our photon propagation code, once a complete calibration of the deployed DeepCore detector has been performed.

### 3.2. Trigger

IceCube DOMs are read out whenever a sufficient number of hits satisfying the hard local coincidence (HLC) condition occur during a pre-defined time window. The HLC condition is satisfied when two or more DOMs in close proximity to one another (nearest or next-nearest neighbors on the same string) register hits within a  $\pm 1 \mu\text{s}$  time window. IceCube uses a simple majority

trigger requiring eight or more DOMs satisfying the HLC condition within a  $5 \mu\text{s}$  time window (this trigger is called “SMT8”). The detector readout is then expanded to a wider  $\pm 10 \mu\text{s}$  time window centered on the trigger time, and includes DOMs which registered hits in the trigger time window but which did not satisfy the HLC condition. These DOMs are said to satisfy the “soft local coincidence” (SLC) condition. Only HLC hits are used by the trigger. Detailed hit information is acquired from DOMs satisfying the HLC condition as these DOMs may have received substantial amounts of light, while less detailed information is acquired from DOMs satisfying the SLC condition as these DOMs typically receive only single photons [13].

To reach lower energies, DeepCore uses an independent SMT3 trigger, with a  $2.5 \mu\text{s}$  time window, applied to DOMs comprising the DeepCore fiducial volume—the DOMs on the strings with HQE DOMs and those on neighboring standard IceCube strings below 2100 m. The background to this trigger from coincident random noise is greatly reduced by application of the HLC condition. Furthermore, the depth of the DOMs suppresses the cosmic-ray background to levels manageable for the DAQ system. The DeepCore SMT3 trigger has an exclusive trigger rate that is  $< 10 \text{ Hz}$ , which is  $< 0.4\%$  that of the standard IceCube SMT8 trigger. Table 1 shows the measured and simulated SMT3 trigger rates from cosmic-rays and atmospheric neutrinos.

Figure 7 shows the fraction of simulated atmospheric  $\nu_\mu$  events satisfying various DeepCore SMT trigger conditions. Since the trigger works only with HLC hits, an event with only three HLC hits can have additional SLC hits. These additional hits will improve the reconstructability of such low multiplicity events. The minimum required multiplicity to reconstruct a track is six, although depending on the distribution of these hits along the strings, unavoidable ambiguities can arise.

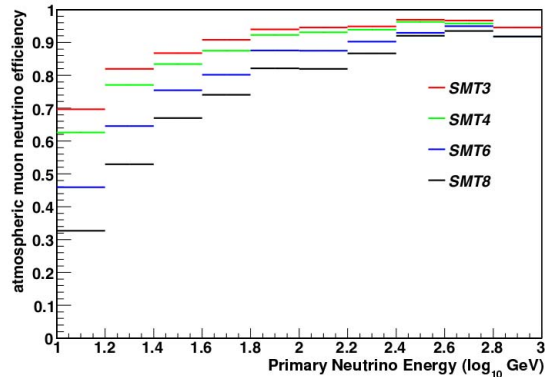


Figure 7: Fraction of simulated atmospheric  $\nu_\mu$  events satisfying different SMT trigger conditions. The SMT3 condition is the loosest and hence admits the highest fraction of low energy events.

Figure 8 shows the effective volume for muon neutrino events,

$$V_{\text{eff}} = V_{\text{gen}} N_{\text{trig}} / N_{\text{gen}}, \quad (1)$$

where  $V_{\text{gen}}$  is the volume in which the events were generated and  $N_{\text{trig}}$  and  $N_{\text{gen}}$  the number of events satisfying the trigger and the number generated, respectively. Figure 8 also shows the effective area,  $A_{\text{eff}}$ , for muon neutrino events satisfying the SMT3 trigger condition as a function of energy. The definition for  $A_{\text{eff}}$  parallels that of  $V_{\text{eff}}$ . Figure 9 shows the effective volume and area for electron neutrinos. To further demonstrate the impact of DeepCore for low energy physics, these figures also show the same quantities as described above but with DeepCore artificially removed in the simulation of the response of the full detector.

Figures 8-9 were all simulated using the 86-string configuration of IceCube (“IC86”) that includes the 15 strings of DeepCore.

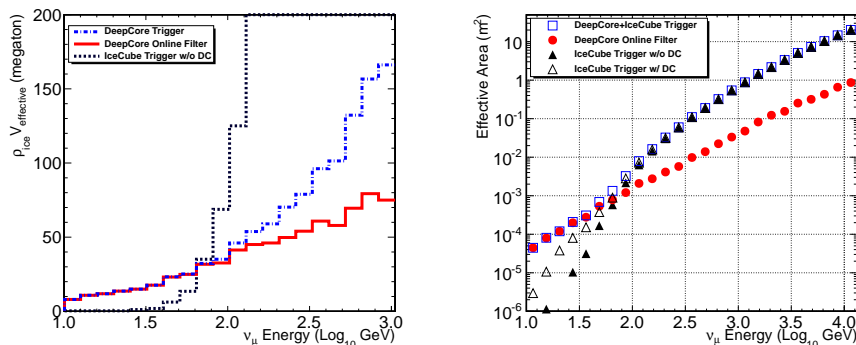


Figure 8: Left: The expected DeepCore muon neutrino effective target mass, the product of the density of ice and the effective volume, after application of the SMT3 trigger (dash-dot line), after application of the online filter (solid line; see Sec. 3.3), after application of the SMT8 trigger for the full 86-string IceCube detector (dotted line) and, to demonstrate the impact of DeepCore, after application of the SMT8 trigger for the IceCube detector simulated *without* DeepCore (dashed line). The hadronic shower at the  $\nu_{\mu}$  interaction vertex can contribute hits and play a role in the triggering and filtering. High energy muon neutrinos that interact and produce a muon outside of the DeepCore volume are typically removed by the filter, eventually causing the solid line in the plot to turn over at energies above those shown. From the DeepCore perspective, such events are indistinguishable from cosmic ray background, although many of them may be selected by the surrounding IceCube detector via other online filters. Right: The expected DeepCore muon neutrino effective area after application of the SMT3 and SMT8 triggers (open squares), after application of the online filter (solid circles; see Sec. 3.3), after application of the SMT8 trigger for the full 86-string IceCube detector (open triangles) and, to demonstrate the impact of DeepCore, after application of the SMT8 trigger for the IceCube detector simulated *without* DeepCore (solid triangles).

More specialized triggers that use data from a combination of IceCube and DeepCore modules are under development to enhance sensitivity to particular signals, such as neutrino signals from solar WIMP annihilations. These specialized triggers include those that can be implemented in the trigger software,

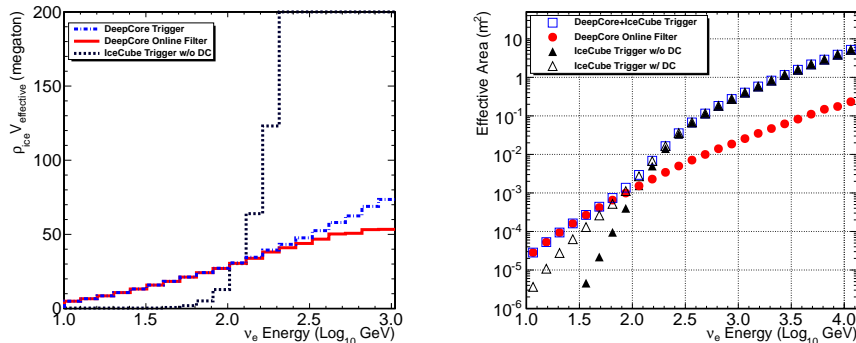


Figure 9: Left: The expected DeepCore electron neutrino effective target mass, the product of the density of ice and the effective volume, after application of the SMT3 trigger (dash-dot line), after application of the online filter (solid line; see Sec. 3.3), after application of the SMT8 trigger for the full 86-string IceCube detector (dotted line) and, to demonstrate the impact of DeepCore, after application of the SMT8 trigger for the IceCube detector simulated *without* DeepCore (dotted line). High energy electron neutrinos that interact outside of the DeepCore volume are typically removed by the filter, causing the solid line in the plot to begin to turn over. Many of these higher energy events may be captured by the surrounding IceCube detector via other online filters. Right: The expected DeepCore electron neutrino effective area after application of the SMT3 trigger (open squares), after application of the online filter (solid circles; see Sec. 3.3), after application of the SMT8 trigger for the full 86-string IceCube detector (open triangles), and, to demonstrate the impact of DeepCore, after application of the SMT8 trigger for the IceCube detector simulated *without* DeepCore (solid triangles).

sensitive to specific event topologies, and those that can be implemented using new hardware operating in conjunction with the existing DAQ system. These triggers will be described in a future publication.

### 3.3. Online Filter

Due to its location at the South Pole, real-time communication with IceCube from the northern hemisphere can only be provided by geosynchronous satellites with limited transmission bandwidth. Since the background flux of cosmic-ray muons is about  $10^6$  times larger than the flux of atmospheric neutrinos in the full IceCube array, individual analyses employ software “filters” that reduce the size of the data sample by selecting likely signal events and removing likely background events. The filtered subset of the triggered data stream is transmitted daily to storage facilities in the north, where more sophisticated reconstruction algorithms are applied to the data. All events are written to portable storage media at the South Pole and transported north for archival storage at the end of each austral winter.

With DeepCore fully deployed and surrounded by standard IceCube strings, a new filter taking full advantage of the vetoing capabilities of the surrounding strings is being used. This new filter is distinct from the standard IceCube filters designed to enrich potential signal relative to background for a variety of event topologies. The design and performance of this filter are described

below. Additional and more sophisticated vetoing algorithms will be applied to filtered data offline in the north. The offline veto algorithms are still under development. Since the cosmic-ray muon flux is attenuated by about an order of magnitude relative to that of IceCube by virtue of DeepCore’s greater average overburden, the overall goal of the trigger, online filter and offline veto is to attain a cosmic-ray muon rejection factor of at least  $10^5$ . At the same time, we aim to maintain a signal efficiency of well over 50% for contained and partially contained neutrino-induced tracks and showers down to  $E_\nu \gtrsim 10$  GeV.

The online filter is used to search for HLC hits in the “veto” region external to DeepCore’s fiducial volume that are consistent with the presence of a downward-going muon. The online filter provides an estimate of the “center of gravity” (COG) and time of the event within DeepCore by calculating the average position  $r$  and time  $t$  of the DOM hits in DeepCore. The initial COG estimate is then refined by using the average position,  $r'$ , of the subset of those hits with times within one standard deviation of the average time. The initial time estimate is refined by using the average of the “corrected” hit times,  $t'$ . Corrected hit times are determined by subtracting from the time of each hit the time that unscattered light would require to travel from the COG at  $r'$ .

With this refined COG estimate, the online filter is used to calculate the speed of a hypothetical particle traveling from each HLC hit in the surrounding IceCube volume (used as a veto region) to the COG. Events that have at least one hit with a speed consistent with  $v = c$ , where the speed  $v = (r' - r_{\text{DOM}})/(t' - t_{\text{DOM}})$ , are rejected. This algorithm is depicted graphically in Fig. 10.

Figure 11 shows the distribution of hypothetical particle speeds per event. The dotted curve depicts the simulated muon background from cosmic-ray air showers using CORSIKA and the solid curve the atmospheric neutrino signal [22]. The atmospheric neutrino events are required to have an interaction vertex inside the DeepCore fiducial volume, as determined from Monte Carlo truth information. The peak for the simulated cosmic-ray muons is slightly above +0.3 m/ns while muons induced by neutrinos in DeepCore mainly give hits with negative particle speeds. Negative speeds indicate that the hypothetical particle traveled outward from the fiducial volume into the veto volume. The peak at positive speeds close to zero is mainly due to early scattered light. By rejecting events with one hit within a particle speed window between +0.25 and +0.4 m/ns we achieve an overall background rejection of roughly  $8 \cdot 10^{-3}$ .

Figure 12 shows the signal efficiency vs. background rejection for events that have one or more hits with a particle speed between +0.25 m/ns and a range of maximum speeds from +0.3 to +1.0 m/ns. As the value of the maximum speed increases, signal efficiency decreases more quickly than background rejection increases. Also taking satellite bandwidth limitations into consideration, we set the maximum allowable speed to +0.4 m/ns. Similarly, varying the minimum speed while holding the maximum speed fixed at +0.4 m/ns, we set the minimum allowable speed to +0.25 m/ns.

As we have enough bandwidth capacity we can effort to send the data with 96% background rejection and keep highest possible signal efficiency. More strict selection criteria start to decrease the signal efficiency, so that we choose

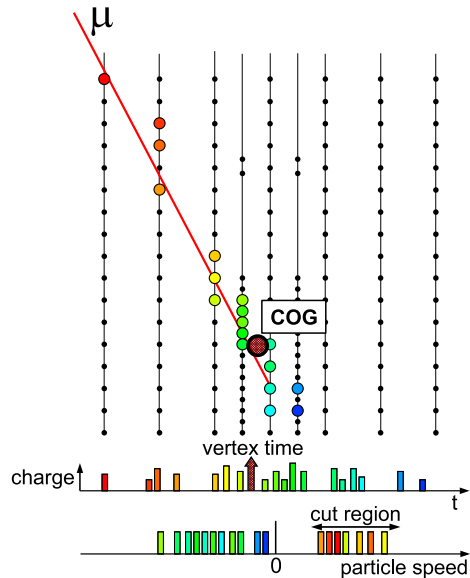


Figure 10: A simulated downward-going muon event that would be vetoed by the algorithm described in the text. The vertical lines represent strings and the small black circles represent individual DOMs. The larger circles at DOM positions represent hits. The earliest hits are in red and the latest in violet, with hit times in between following the colors of the rainbow. The center of gravity of the hits in the DeepCore volume is labelled COG. The hits in the upper left hand side, colored red and orange, are the early hits associated with the muon’s entry point into the detector fiducial volume, and these hits have associated “particle speeds” consistent with speed of light travel between the hit and the COG, and therefore are consistent with having been produced by a muon. These hits enter the “cut region” in particle speed, shown at the bottom of the figure, and the event is vetoed on this basis.

0.4m/ns as selection cut.

The background rejection and signal detection rates of the online filter are compiled in Table 1. For IceCube in its 79-string configuration, the online filter passed data at about 4 GB/day, about 5% of the available satellite bandwidth allocated to IceCube.

The effect of the online filter on the muon neutrino effective volume and effective area is shown in Fig. 8. Its effect for electron neutrinos is shown in Fig. 9.

The analysis of the first year of IceCube DeepCore data is underway. One of the first analyses nearing completion is a measurement of hadronic and electromagnetic showers induced by atmospheric neutrinos in the DeepCore fiducial volume [23]. In Fig. 13, two candidate shower events with energies on the order of  $10^2$  GeV (left) and  $10^3$  GeV (right) are shown. These events were extracted from the data after application of the triggering and filtering criteria described above, along with a variety of additional, more sophisticated selection criteria.



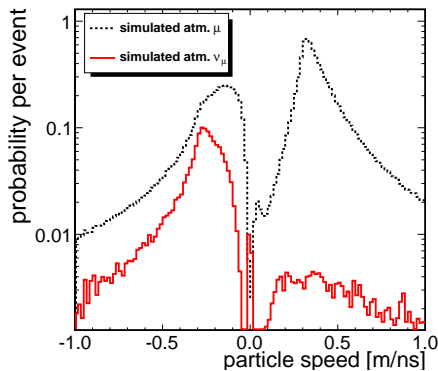


Figure 11: Particle speed probabilities per event for simulated muons from cosmic-ray interactions (black dashed line) and simulated muons from atmospheric neutrinos inside DeepCore (red solid line). The speed is defined to be positive if the hit occurred before the COG time (see text) and negative if it appeared after. Hits in the veto region are generally expected to have a speed close to  $c \simeq +0.3$  m/ns. Smaller speeds occur for light delayed by scattering. Larger speeds are in principle acausal, but since the COG time represents the start of a DeepCore event, whereas the COG position defines its center, the particle speeds for early hits are slightly overestimated. Events with a hit within a particle speed window between +0.25 and +0.4 m/ns are rejected.

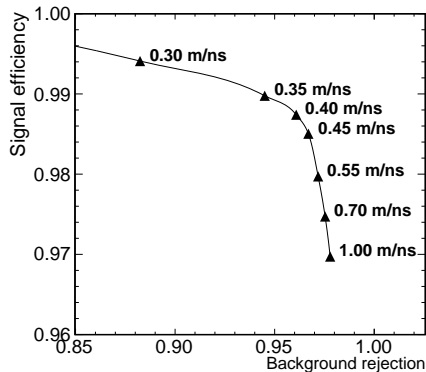


Figure 12: Signal efficiency as a function of background rejection for events having one or more hits with a particle speed (see text) between +0.25 m/ns and a variety of upper values, ranging from +0.35 m/ns to +1.0 m/ns, as indicated in the figure. Upper values higher than about +0.4 m/ns result in greater signal loss without significant additional background rejection.

Table 1: Data and signal passing rates (in Hz) after application of the DeepCore trigger and online filter. In anticipation of future selection criteria that will require reconstructed interaction vertices to be well contained in the DeepCore fiducial volume, only atmospheric neutrinos interacting inside the detector fiducial volume (a cylinder of radius 200 m and height 350 m) were simulated. The online filter has negligible impact on simulated signal events while reducing the data, which is dominated by downward-going muons, by about a factor of 15 relative to the SMT3 trigger. The data used here came from the 79-string configuration of IceCube (“IC79”) while the simulated signal used the 86-string configuration of IceCube (“IC86”). Numbers for the data in IC86 running will be marginally higher than those shown here.

Rates (Hz)	Data (IC79) (annual average)	Atm. $\nu_\mu$ (IC86) (Bartol [22]) (↑: upward) (↓: downward)	Atm. $\nu_e$ (IC86) (Bartol [22]) (↑: upward) (↓: downward)
All IceCube Triggers	1900		
DeepCore SMT3 Trigger	185 (9.7%)	$3.59 \cdot 10^{-3}$ (100%) (↑: $1.54 \cdot 10^{-3}$ ) (↓: $2.05 \cdot 10^{-3}$ )	$0.793 \cdot 10^{-3}$ (100%) (↑: $0.411 \cdot 10^{-3}$ ) (↓: $0.382 \cdot 10^{-3}$ )
DeepCore Online Filter	17.5 (0.9%)	$3.57 \cdot 10^{-3}$ (99.4%) (↑: $1.53 \cdot 10^{-3}$ ) (↓: $2.04 \cdot 10^{-3}$ )	$0.789 \cdot 10^{-3}$ (99.5%) (↑: $0.409 \cdot 10^{-3}$ ) (↓: $0.380 \cdot 10^{-3}$ )

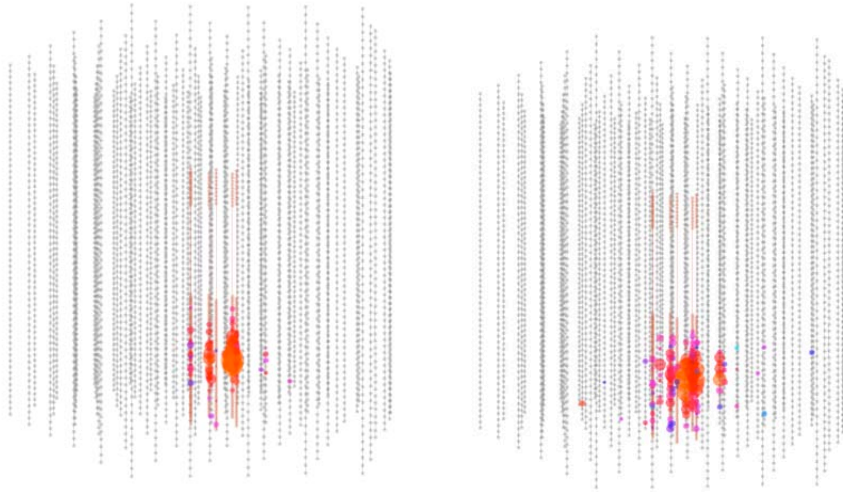


Figure 13: Two candidate shower events induced by atmospheric neutrino interactions in the DeepCore fiducial volume. The event energies are on the order of  $10^2$  GeV (left) and  $10^3$  GeV (right). Each black point represents a single DOM. Points with superimposed colored circles represent DOMs that received light associated with the event, with the size of the circle proportional to the amount of light, and the color indicating the relative time of arrival of the first photon detected by that DOM, with red earliest and violet latest (following the colors of the rainbow).

#### 4. Conclusions

The IceCube DeepCore sub-array has been deployed and is actively taking analysis-quality physics data. It was designed to be sensitive to neutrino energies as low as about 10 GeV, over an order of magnitude lower than the original goal for IceCube. Situated in the very clear ice more than 2100 m below the surface, outfitted with new high quantum efficiency photomultiplier tubes, and deployed on a very close spacing, DeepCore is operating as anticipated and is expected to reach its low energy goal. We have successfully implemented simple and robust online algorithms that reduce the background level by over two orders of magnitude while retaining most of the expected neutrino signal. More sophisticated algorithms, run offline in the north, should allow us to further reduce the background to a level comparable to the atmospheric neutrino flux. This should give DeepCore sensitivity to a wide range of exciting physics, from low mass solar WIMP annihilations and atmospheric neutrino oscillations to soft-spectrum point sources of neutrinos in the southern sky and exotic physics such as slow-moving monopoles.

## 5. Acknowledgements

We acknowledge the support from the following agencies: U.S. National Science Foundation-Office of Polar Programs, U.S. National Science Foundation-Physics Division, University of Wisconsin Alumni Research Foundation, the Grid Laboratory Of Wisconsin (GLOW) grid infrastructure at the University of Wisconsin - Madison, the Open Science Grid (OSG) grid infrastructure; U.S. Department of Energy, and National Energy Research Scientific Computing Center, the Louisiana Optical Network Initiative (LONI) grid computing resources; National Science and Engineering Research Council of Canada; Swedish Research Council, Swedish Polar Research Secretariat, Swedish National Infrastructure for Computing (SNIC), and Knut and Alice Wallenberg Foundation, Sweden; German Ministry for Education and Research (BMBF), Deutsche Forschungsgemeinschaft (DFG), Research Department of Plasmas with Complex Interactions (Bochum), Germany; Fund for Scientific Research (FNRS-FWO), FWO Odysseus programme, Flanders Institute to encourage scientific and technological research in industry (IWT), Belgian Federal Science Policy Office (Belspo); University of Oxford, United Kingdom; Marsden Fund, New Zealand; Japan Society for Promotion of Science (JSPS); the Swiss National Science Foundation (SNSF), Switzerland; A. Gro acknowledges support by the EU Marie Curie OIF Program; J. P. Rodrigues acknowledges support by the Capes Foundation, Ministry of Education of Brazil.

## References

- [1] A. Achterberg, et al., First Year Performance of the IceCube Neutrino Telescope, *Astropart. Phys.* 26 (2006) 155–173.
- [2] R. Abbasi, et al., *Phys. Rev. Lett.* 102 (2009) 201302.
- [3] M. Bissok, D. Boersma, J.-P. Huelss, C. Rott, Search for Dark Matter in the Milky Way with IceCube, to be published in Proceedings of the 32nd International Cosmic Ray Conference, Beijing.
- [4] R. Abbasi, et al., *Phys. Rev. D* 84 (2011) 022004.
- [5] O. Mena, I. Mocioiu, S. Razzaque, *Phys. Rev. D* 78 (2008) 093003.
- [6] I. Taboada, Multiflavor and Multiband Observations of Neutrinos from Core Collapse Supernovae, *Phys. Rev. D* 81 (8) (2010) 083011.
- [7] V. Baum, L. Demirörs, L. Köpke, M. Ribordy, et al., Supernova Detection with IceCube and Beyond, to be published in Proceedings of the 32nd International Cosmic Ray Conference, Beijing.
- [8] L. Demirörs, M. Ribordy, M. Salathe, Novel Technique for Supernova Detection with IceCube, [arXiv:1106.1937v2](https://arxiv.org/abs/1106.1937v2).
- [9] I. F. M. Albuquerque, G. Burdman, Z. Chacko, Direct Detection of Supersymmetric Particles in Neutrino Telescopes, *Phys. Rev. D* 75 (3) (2007) 035006.
- [10] I. F. M. Albuquerque, S. R. Klein, Supersymmetric and Kaluza-Klein Particles Multiple Scattering in the Earth, *Phys. Rev. D* 80 (1) (2009) 015015.
- [11] J. Bahcall, P. Mészáros, *Phys. Rev. Lett.* 85 (2000) 1362.
- [12] R. Abbasi, et al., Calibration and Characterization of the IceCube Photomultiplier Tube, *Nucl. Inst. Meth. A* 618 (1-3) (2010) 139–152.
- [13] R. Abbasi, et al., The IceCube Data Acquisition System: Signal Capture, Digitization, and Timestamping, *Nucl. Inst. and Meth. A* 601 (2009) 294–316.
- [14] M. Ackermann, et al., Optical Properties of Deep Glacial Ice at the South Pole, *J. Geophys. Res.* 111 (2006) D13203.
- [15] P. Price, et al., Temperature Profile for Glacial Ice at the South Pole: Implications for Life in a Nearby Subglacial Lake, Proceedings of the National Academy of Sciences 99 (12) (2002) 7844–7847.
- [16] A. Karle, IceCube: Construction Status and First Results, *Nucl. Inst. Meth. A* (604) (2009) S46–S52.

- [17] D. Heck, et al., CORSIKA: A Monte Carlo Code to Simulate Extensive Air Showers, Tech. Rep. FZKA 6019 (1998) 1–90.
- [18] A. Gazizov, M. Kowalski, ANIS: High Energy Neutrino Generator for Neutrino Telescopes, Comput. Phys. Commun. 172 (2005) 203–213.
- [19] C. Andreopoulos, et al., The GENIE Neutrino Monte Carlo Generator, Nucl. Instrum. Meth. A614 (2010) 87–104.
- [20] D. Chirkin, W. Rhode, Propagating Leptons Through Matter with Muon Monte Carlo (MMC)[arXiv:hep-ph/0407075v2](https://arxiv.org/abs/hep-ph/0407075v2).
- [21] J. Lundberg, et al., Light Tracking Through Ice and Water - Scattering and Absorption in Heterogeneous Media with PHOTONICS, Nucl. Inst. Meth. A581 (2007) 619–631.
- [22] G. D. Barr, et al., Phys. Rev. D 70 (2004) 023006.
- [23] C. H. Ha, D. J. Koskinen, et al., Observation of Atmospheric Neutrino-Induced Cascades in IceCube-DeepCore, to be published in Proceedings of the 32nd International Cosmic Ray Conference, Beijing.